1-1-2016

Preparation and Characterization of Photoactive Antimicrobial Graphitic Carbon Nitride (g-C_3N_4) Films

John H. Thurston
College of Idaho

Necia M. Hunter
College of Idaho

Kenneth A. Cornell
Boise State University

RSC Adv., 2016, **6**, 42240-42248
DOI: 10.1039/C6RA05613J
Received 02 Mar 2016, Accepted 18 Apr 2016
First published online 20 Apr 2016

Preparation and characterization of photoactive antimicrobial graphitic carbon nitride (g-C_3N_4) films

John H. Thurston[a,], Necia M. Hunter[a], Kenneth A. Cornell[b]*

[a]Department of Chemistry, The College of Idaho, 2112 Cleveland Blvd, Caldwell, ID 83605

[b]Department of Chemistry and Biochemistry, Boise State University, Boise, ID 83725

Abstract

Photoactive films derived from nanostructured samples of the metal-free, intermediate band gap semiconductor graphitic carbon nitride (ns-*g*-C_3N_4) have been synthesized and characterized for their particle properties and antimicrobial activity. Physical characterization reveals that these materials are composed of discrete nanoparticles whose dimensions range from 200 nm to 700 nm. Investigation of the photochemical reactivity of ns-*g*-C_3N_4 using coumarin-3-carboxylic acid (3-CCA) indicates that this material produces reactive oxygen species (ROS) under visible radiation. When irradiated with 0.31J visible light, ns-*g*-C_3N_4-based materials reduced the viability of both gram-negative *Escherichia coli* O157:H7 and gram-positive *Staphylococcus aureus* by approximately 50%. Nearly complete inactivation of both strains of microorganisms was achieved upon administration of a 0.62J dose of visible radiation. Importantly, no biocidal activity was observed for non-irradiated samples, indicating that the *g*-C_3N_4-derived films are not

inherently toxic in the absence of visible light. The results of this study suggest that materials and, by extention, films and coatings derived from *g*-C_3N_4 may present a novel route for controlling pathogenic microorganisms on surfaces in the environment, and could be useful in reducing incidents of hospital-acquired infections.

Introduction

The acquisition of antibiotic-sensitive and antibiotic-resistant nosocomial infections are correlated with an overall increase in patient morbidity and mortality, and responsible for annual treatment costs of approximately $9.8 billion.[1] It is estimated that there are 440,000 cases of drug-resistant nosocomial infections among the U.S. adult population each year.[1]

Of particular concern in hospital-acquired infections is the potential of solid surfaces to serve as reservoirs of pathogenic microorganisms. This is particularly true for surfaces with high touch frequencies, such as door handles, bed rails, and toilet seats.[2] A variety of gram-positive bacteria, including vancomycin-resistant *Enterococcus* (VRE) and methicillin-resistant *S. aureus* (MRSA), have been reported to survive for months on dry surfaces.[3] The same study reported that gram-negative species (*E. coli, Klebsiella* spp.) and the fungal pathogen *Candida albicans* also survived on dry surfaces for extended periods of time.[3] Similarly, wet surfaces, including bedding, ultrasonic nebulizers and ventilation grills have been observed to function as environmental reservoirs for MRSA.[2]

The mechanism by which environmental reservoirs facilitate microbial transmission in a hospital setting remains the subject of much study.[4] In the case of VRE, it has been reported that touching a contaminated surface can result in microbial transfer with approximately the same frequency as contact with a colonized patient.[4] Reports have also shown that environmental decontamination is able to successfully suppress outbreaks of MRSA and VRE.[4] Consequently, there is a clear

incentive to develop new technologies for surface decontamination to reduce the incidence of hospital-acquired infections or biofilm formation.

A wide variety of materials, including wide band gap semiconductors[5, 6], silver-based materials[7], antimicrobial polymers[8] and biopolymers[9-11], carbon nanotubes[12, 13] and functionalized clays[5, 14] have been used to produce novel antimicrobial coatings. Among these technologies, narrow or intermediate band gap semiconductors that photo-catalytically generate cytotoxic reactive oxygen species (ROS) from molecular oxygen show particular promise for the reduction of bacterial populations in interior environments.[15, 16] Graphitic carbon nitride (*g*-C_3N_4) is an emerging metal-free, intermediate band gap semiconductor.[17-20] This material is particularly attractive for environmental remediation applications due to the fact that *g*-C_3N_4 based materials have been shown to produce a variety of ROS in solution[21-25], are resistant to photo-bleaching, and are stable under repeated electronic cycling while also being photo-responsive to visible wavelengths of electromagnetic radiation.[24]

The potential biocidal or antimicrobial utility of *g*-C_3N_4 is poorly explored. Two studies have described the antimicrobial properties of composite *g*-C_3N_4 complexes containing either monoclinic sulfur or Ag_2CO_3.[26, 27] Two additional studies detail the ability of g-C_3N_4 to promote the solution-state disinfection of single strains of microorganisms.[28, 29] However, all of these reports have relied on aqueous suspensions of the g-C_3N_4 materials to achieve the reported antimicrobial effects. Surprisingly, there have been no studies exploring the utility of *g*-C_3N_4 for the fabrication of biocidal surfaces or surface coverings or coatings, an application for which this material appears to be uniquely suited. In addition, the ability of *g*-C_3N_4 to exhibit demonstrable activity against both gram-positive and gram-negative microorganisms has yet to be established. Herein we describe the synthesis and physical characterization of nanostructured samples of *g*-

C_3N_4 as well as the results of studies demonstrating visible–light driven antimicrobial activity of *g*-C_3N_4-derived films against the clinically relevant microbes *S. aureus* and *E. coli* O157:H7.

Experimental

Reagents. All chemicals and media components were either purchased from Sigma-Aldrich Corp. (St. Louis, MO) or from Fisher Scientific (Pittsburgh, PA). Pure strain samples of *E. coli* O157:H7 (ATCC #43894) and *S. aureus* (ATCC #6538) were purchased from the ATCC (Mannassas, VA) and were grown using Luria Bertani (LB) broth or agar.

Preparation of *g*-C_3N_4: Samples of *g*-C_3N_4 were prepared by a slight modification of the reported procedures.[22, 24, 30] Briefly, 2.0 g of dicyandiamide was placed in a porcelain crucible and heated from 25°C to 575°C at a rate of 175°C/hour in a muffle furnace. The sample dwelled at 575°C for four hours and then was cooled to ambient temperature over 18 hours. The resulting yellow solid was ground to free flowing powder in an agate mortar and pestle prior to analysis and additional modification.

Preparation of nanostructured *g*-C_3N_4: Samples of nanostructured *g*-C_3N_4 (ns-*g*-C_3N_4) were prepared using a modification of the protocol reported by Yang *et al*.[31] A 200mg portion of bulk *g*-C_3N_4 powder was suspended in 20 mL of 2-propanol and the resulting mixture was subjected to sonication at room temperature for 24 hours. After 24 hours, 20 mL of 0.9% saline solution was added to the mixture and the alcoholic solvent removed *via* azeotropic distillation to produce a 10 mg/mL aqueous suspension of nanostructured *g*-C_3N_4.

Spectroscopic characterization of *g*-C_3N_4 and ns-*g*-C_3N_4: Infrared spectra were collected on a Thermo-Nicolet Avatar 360 FT-IR spectrophotometer equipped with a single reflection Smart Orbit diamond ATR aperture in the range of 4000 – 400 cm^{-1}. Fluorescence spectra were collected on a Varian Cary Eclipse Fluorescence spectrophotometer. Diffuse reflectance UV-Vis spectroscopy measurements were collected on powder samples using a Cary 5000 spectrophotometer. Bandgap values are estimated using Kubelka-Munk theory.[32, 33] Raman data

was collected on a Thermo Nicolet 870 instrument that was coupled to an FT-Raman module. X-ray photoelectron spectroscopy was conducted on a PHI 5000 Versaprobe II Scanning ESCA microprobe using a monochromatic Al K_α X-ray source (1486.6 eV). The base vacuum in the chamber was better than 1.5 x 10^{-10} torr. The samples used in this study were probed by an X-ray source with a power of 100W and a beam diameter of 150μm. Survey scans were collected on several different areas to study the relative composition of the sample. High resolutions scans were performed on each elemental region to improve the signal-to-noise ratio. Sample charging effects were minimized using a low energy electron gun and Ar^+ ions. The binding energy scale was referenced to the C1s peak (284.8 eV) to accommodate peak shifts as a consequence of sample charging effects.

Physical characterization of *g*-C_3N_4 and ns-*g*-C_3N_4: Secondary electron images of *g*-C_3N_4 and ns-*g*-C_3N_4 were recorded on a Hitachi S-3400N analytical scanning electron microscope operating at an accelerating potential of 10.0 kV. Samples were prepared by dispersing the powder on adhesive carbon tapes and sputter coating with chromium to prevent charging and to increase contrast. The hydrodynamic radius of the materials developed for this study was measured using dynamic light scattering (DLS) measurements on a Zetasizer Nano ZS Zetapotential/Particle size analyzer (Malvern Instruments) equipped with a monochromatic and coherent light beam (633 nm He-Ne laser, 4 mW). Powdered samples of *g*-C_3N_4 or ns-*g*-C_3N_4 were dispersed in deionized water to get a pre-determined concentration of 0.001 wt% aqueous solution. The samples used for analysis were subjected to ultrasonication for about 10 mins and immediately transferred to zeta cell for measurements. The particle size scans were averaged to obtain size distribution data. Powder x-ray diffraction data was collected on a Rigaku Miniflex 600 powder x-ray diffractometer

using Cu K_α radiation (graphite monochromator, $\lambda = 1.5418$ Å). Data was collected between 2.0° and 65.0° on 2θ with a step size of 0.01°.

Irradiation procedures: Irradiation experiments were carried out by illuminating the sample mixture with an ozone free xenon light source operating at 270 W (Power source: Newport # 69911). The lamp housing (Newport # 67001) contained an F/2.2 fused silica condenser and rear reflector (1.6 correction factor). The photon flux was stripped of infra-red radiation using a temperature-controlled, recirculating water filter. Similarly, UV radiation was removed using a λ = 400 nm cut-off filter (Oriel # FSQ-GG400). Total radiation doses were estimated using an average source irradiance of 30 $mW \cdot m^{-2} \cdot nm^{-1}$ (working distance = 0.5 m), a collimated beam diameter of 33 mm, and applying equations 1-3.

$$\text{Radiant Exitance } (W \cdot m^{-2}) = M_e = 1.6 \times 0.05 \times \frac{30mW}{m^2 \cdot nm} \int_{\lambda_1}^{\lambda_2} d\lambda \qquad \text{Equation 1}$$

$$\text{Radiant Power } (W) = \varphi_e = A \times M_e \qquad \text{Equation 2}$$

$$\text{Total Radiant Dose } (J) = \text{Radiant Energy } (J) = \varphi_e \times t \qquad \text{Equation 3}$$

The variables A and t represent the incident beam area (m^2) and irradiation time (s), respectively. Only incident radiation whose wavelengths fell in the spectral window between the UV cutoff filter (λ_1 = 400 nm) and the experimentally determined band gap of the semiconductor (λ_2 = 442 nm) were used in the dose calculations.

Determination of ROS production: A 200mg sample of ns-*g*-C_3N_4 was suspended in 20 mL 2 mM coumarin-3-carboxylic acid in 0.9% saline.[34] The sample was stirred at 260 rpm and the mixture was either covered (dark control) or subjected to visible radiation. Aliquots of the reaction

mixture and dark control were collected prior to the start of irradiation (t = 0) and periodically throughout the experiment (t = 1, 2, 4 hr). The photocatalyst was removed from the reaction mixture by centrifugation at 10,000 x g for 10 minutes and passage through a syringe filter (0.2 μm). The fluorescence intensity of the resulting solution was measured at 450 nm using an excitation wavelength of 395 nm (1.5nm slit) and an emission scan of 400-500 nm.

Antimicrobial experiments: Several isolated colonies of either *E. coli* O157:H7 or *S. aureus* cultures grown overnight on LB agar were suspended in 5 mL 0.9% sterile saline. The volume of the suspension was adjusted to bring the final absorbance (600 nm) to 0.5. The resulting solution was serially diluted to 10^{-6} using ice-cold sterile saline.[35] A 1.0 mL portion of the 10^{-6} dilution was combined with 20 mL of sterile 0.9% saline containing 20 mg ns-*g*-C_3N_4 and the resulting mixture vacuum filtered onto a 0.45 μm nitrocellulose filter disk (47 mm disk diameter). These experimental conditions resulted in a bacterial loading densities of ~11.4 CFU/cm^2 (*E. coli* O157:H7) and ~14.4 CFU/cm^2 (*S. aureus*). In all cases, the microbial loading density was selected to be 4-5 times higher than the average density of MRSA reported to be present on elevated surfaces in a hospital environment (~3.5 CFU/cm^2).[36] To measure nonspecific cytotoxicity (*e.g.* heating effects), replicate filters were prepared that contained bacteria, but lacked ns-*g*-C_3N_4.

Prior to irradiation, inoculated nitrocellulose filter disks were placed on pieces of sterile saline-dampened Whatman #1 filters in a glass petri dish. The filters were irradiated for 0, 30, 60, or 120 minutes (~0-0.68 J applied radiation). Controls consisted of similarly prepared filters that received no irradiation (dark control), or similarly irradiated/non-irradiated inoculated filters lacking ns-*g*-C_3N_4. The glass petri dish was placed on ice during the irradiation to minimize cell killing due to direct sample heating. After irradiation, the nitrocellulose filter disk was placed on LB agar and

incubated for 24 hrs at 37°C. After the incubation period, colony forming units (CFU) on the disk were counted manually, and the % total CFU calculated using the formula:

$$\%\ \text{Total CFU} = \frac{\text{Test CFU}}{\text{Total CFU (t=0)}} \times 100 \qquad \text{Equation 4}$$

Each experiment was performed three times, with each time point tested in triplicate. The results of the experiments are expressed as the mean % total CFU ± SEM (standard error on the mean). In all cases, the experiments were stopped when the colony count dropped below 2.5 CFU/cm^2, an accepted threshold for the decontamination of high touch frequency sites.[37]

Results and Discussion

Preparation of ns-*g*-C_3N_4

Bulk samples of *g*-C_3N_4 were prepared by direct thermal polymerization of the molecular precursor dicyandiamide in a manner similar to procedures described elsewhere.[30] The successful formation of the desired graphitic phase of carbon nitride was confirmed by powder X-ray diffraction experiments (Figure 1). In particular, the peak at 2θ = 27.5° corresponds to the interlayer spacing (d = 3.24Å) for *g*-C_3N_4, while a second peak observed at 2θ = 12.7° closely matches the dimensions expected for the spacing of the individual melon subunits present in the polymeric material (d = 6.94Å).

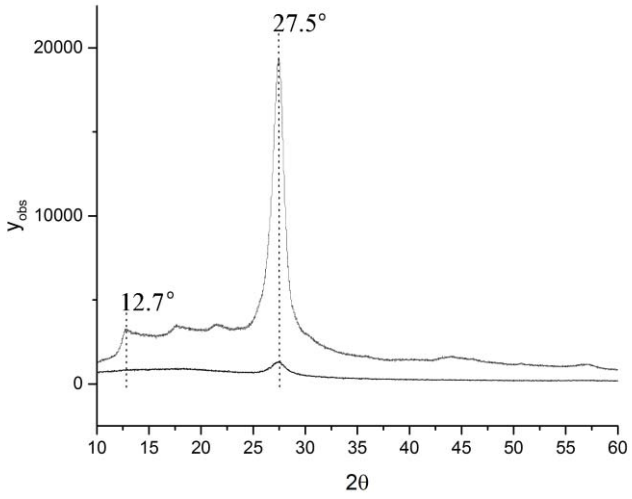

Figure 1: Powder X-ray diffraction data for samples of *g*-C_3N_4 (top trace) and ns-*g*-C_3N_4 (bottom trace). Peaks observed at 2θ = 27.5° and 12.7° are consistent with interlayer spacing and individual melon subunit spacing, respectively, for the material.

Post-synthesis modification of *g*-C_3N_4 using either physical or chemical techniques has been previously reported to produce nanostructured samples of the material (ns-*g*-C_3N_4).[31] As part of this study, we have explored the formation of antimicrobial films from ns-*g*-C_3N_4 on the basis of two principle considerations: First, the reduced particle size is anticipated to facilitate the formation of materials with an overall improved degree of structural homogeneity. Second, the smaller particle size present in the exfoliated samples will favor charge carrier migration to the semiconductor surface over deleterious recombination events.[15] This, in turn, is anticipated to result in enhanced photochemical activity and quantum efficiency of these systems, with respect to the desired antimicrobial applications.

Samples of ns-*g*-C_3N_4 used in this study were produced by means of a sonication-induced exfoliation process. The effects of exfoliation on the structure and morphology of *g*-C_3N_4 were investigated by powder X-ray diffraction and scanning electron microscopy, and the

hydrodynamic radius of the materials before and after the sonication process were compared. As shown in Figure 1, the strong reflection centered at $2\theta = 27.5°$ arising from the interlayer spacing of the bulk material is also observed in samples of ns-*g*-C_3N_4, indicating that the lamellar structure of the material is conserved through the exfoliation process. Investigation of the morphology of the materials by scanning electron microscopy revealed that bulk *g*-C_3N_4 consists principally of large, extended layers (Figure 2-A). In contrast, as illustrated in Figure 2-B, samples that have been subjected to sonication are observed to be composed of discrete particles with dimensions ranging from approximately 200 - 700 nm. The results of the electron microscopy analysis correlate well with the experimentally measured hydrodynamic radius of samples of the bulk and exfoliated *g*-C_3N_4. Bulk g-C_3N_4 consisted of approximately 66.7% particles with dimensions of 1.48 ± 0.51 μm (inset Figure 2-A). In contrast, analysis of ns-g-C_3N_4 revealed that 90% of the samples were composed of particles with dimensions of 419 ± 198 nm (inset Figure 2-B).

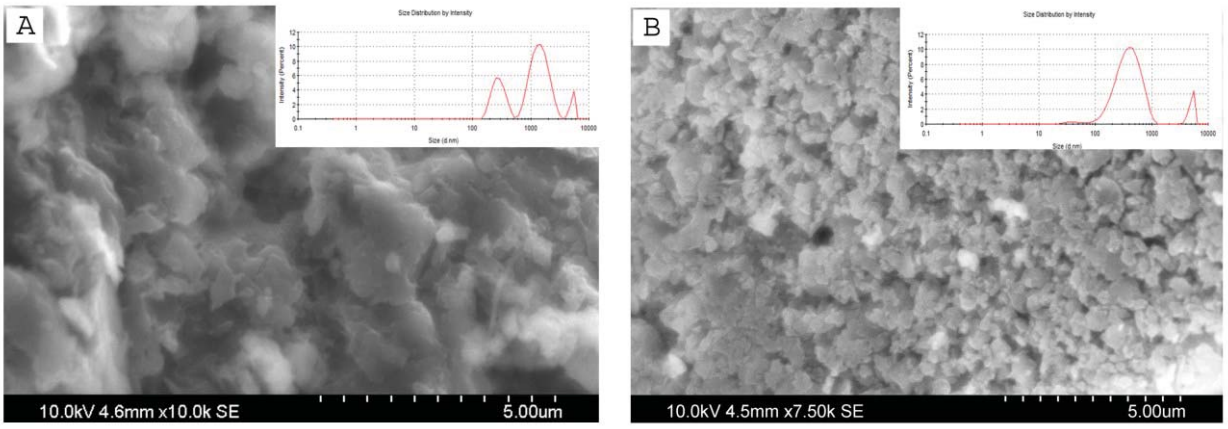

Figure 2: Scanning electron micrographs detailing the morphology of samples of (A) *g*-C_3N_4 (10.0k magnification) and (B) ns-*g*-C_3N_4 (7.50k magnification) produced through sonication induced exfoliation of the bulk material in 2-propanol. Inset images detail the relative particle size distribution as observed through hydrodynamic radius measurements.

The chemical composition of the ns-*g*-C_3N_4 was investigated by absorbance spectroscopy (FT-IR and Raman) and x-ray photoelectron spectroscopy (XPS). The FT-IR spectrum of both the bulk *g*-C_3N_4 and exfoliated ns-*g*-C_3N_4 demonstrated the characteristic vibrational and breathing

modes associated with the heptazine subunits and the terminal amine functional groups present in the extended structure of *g*-C_3N_4 (Figure 3, *left*). The sharp absorbance observed at 808 cm^{-1} may originate from either *s*-triazine or from heptazine ring units, while the numerous peaks found between 900 cm^{-1} and 1800 cm^{-1} are in excellent agreement with reported data for samples of *g*-C_3N_4 produced *via* thermal polymerization reactions.[22, 38] One notable exception is the strong absorbance peak observed at 1402 cm^{-1}. This peak has previously been attributed to the presence of *s*-triazine (C_3N_3) in the material, which suggests that the initial bulk materials were incompletely condensed.[39] It is notable that the relative intensity of the absorbance peak at 1402 cm^{-1} decreases significantly in the exfoliated samples, suggesting that the sonication employed in the fabrication of the ns-*g*-C_3N_4 promotes additional aggregation and condensation of residual *s*-triazine units that were present in the bulk material.

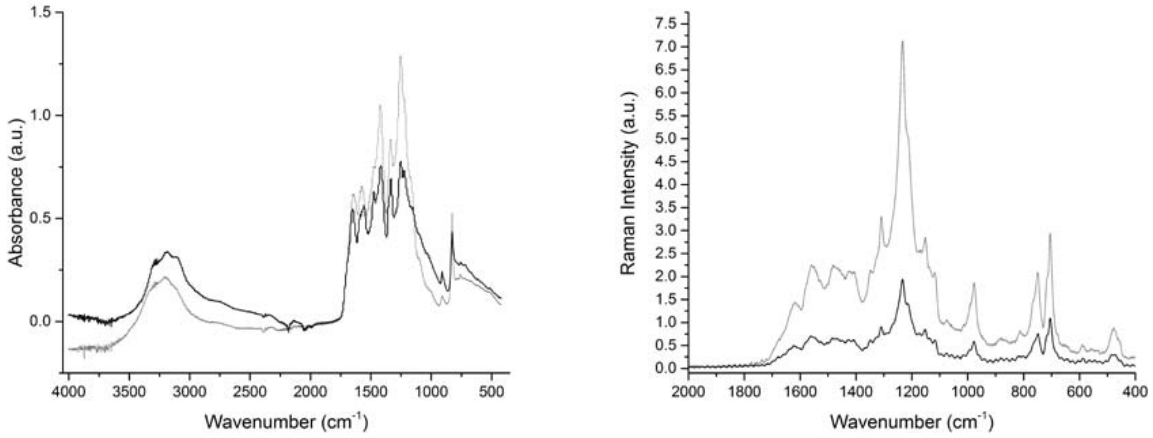

Figure 3: Fourier transform infrared (FTIR) absorbance spectrum (left) and Raman spectrum (right) of *g*-C_3N_4 produced via thermal polymerization of dicyandiamide (grey) and ns-*g*-C_3N_4 produced via sonication induced exfoliation of the bulk material (black). The spectra reveal a general conservation of structure and composition in forming ns-*g*-C_3N_4 from *g*-C_3N_4.

The results of the FT-IR experiments are supported by Raman spectroscopy (Figure 3, *right*). Raman spectroscopy has been widely used to assess the internal structure of carbon-based

materials.[40] In this case, the peak at approximately 1600cm^{-1} (*G* mode) can be attributed to vibrations arising from sp^2 hybridized carbon atoms. In contrast, the peak at 1350cm^{-1} (*D* mode) is a product of vibrations arising from sp^3 hybridized carbon centers.[39] These sp^3 hybridized carbon centers are not associated with the accepted structure of *g*-C_3N_4 and can be viewed as defects in the lamellar structure of the complex. Consequently, the ratio of the Raman peak intensity (I_D/I_G) can serve as a measure of the evolution of the relative structural disorder in the material as a consequence of the initial polymerization and subsequent exfoliation process. In this case, the I_D/I_G ratio for the bulk material was calculated to be 1.66, whereas the I_D/I_G ratio for the exfoliated samples of ns-*g*-C_3N_4 was 1.42. These ratios support the results of the FT-IR analysis and suggest that samples of ns-*g*-C_3N_4 have a smaller number of interstitial defects relative to the bulk materials. These results are consistent with an exfoliation-and-regrowth mechanism that has previously been proposed for the formation of nanostructured *g*-C_3N_4 materials.[39]

The effects of the sonication process on the composition of the *g*-C_3N_4 samples were investigated by X-ray photoelectron spectroscopy (XPS). In particular, we sought to confirm that the formation of ns-*g*-C_3N_4 did not fundamentally alter the chemical composition of the material or introduce additional functional groups that could negatively impact the biological compatibility of the materials. As illustrated in Figure 4, bulk samples of *g*-C_3N_4 contain a single significant carbon environment with a binding energy of 288.3 eV. This peak is consistent with sp^2 hybridized carbon centers in nitrogen-containing aromatic rings (N-*C*=N). This peak is effectively unchanged in the nanostructured sample (288.4 eV). A second, significant peak correlating to adventitious graphitic carbon contamination (sp^2 C-C) is also observed in samples of ns-*g*-C_3N_4. This peak may be observed as a consequence of the solution-based synthetic methodology employed in the fabrication of these materials as part of this study. The N 1s spectrum of bulk and ns-*g*-C_3N_4 has

been resolved into three components with binding energies of 398.8 eV (sp^2 C=*N*-C), 400.3 eV (N(3)) and 401.3 eV (conjugated N-H chemical environment), respectively. The relative intensity of the N-H peak decreases in moving from the bulk to the nanostructured material, while the intensity of the N(3) peak simultaneously increases. This data further reinforces the FT-IR results, suggesting that sonication of bulk *g*-C_3N_4 facilitates additional condensation and internal organization of the extended material.

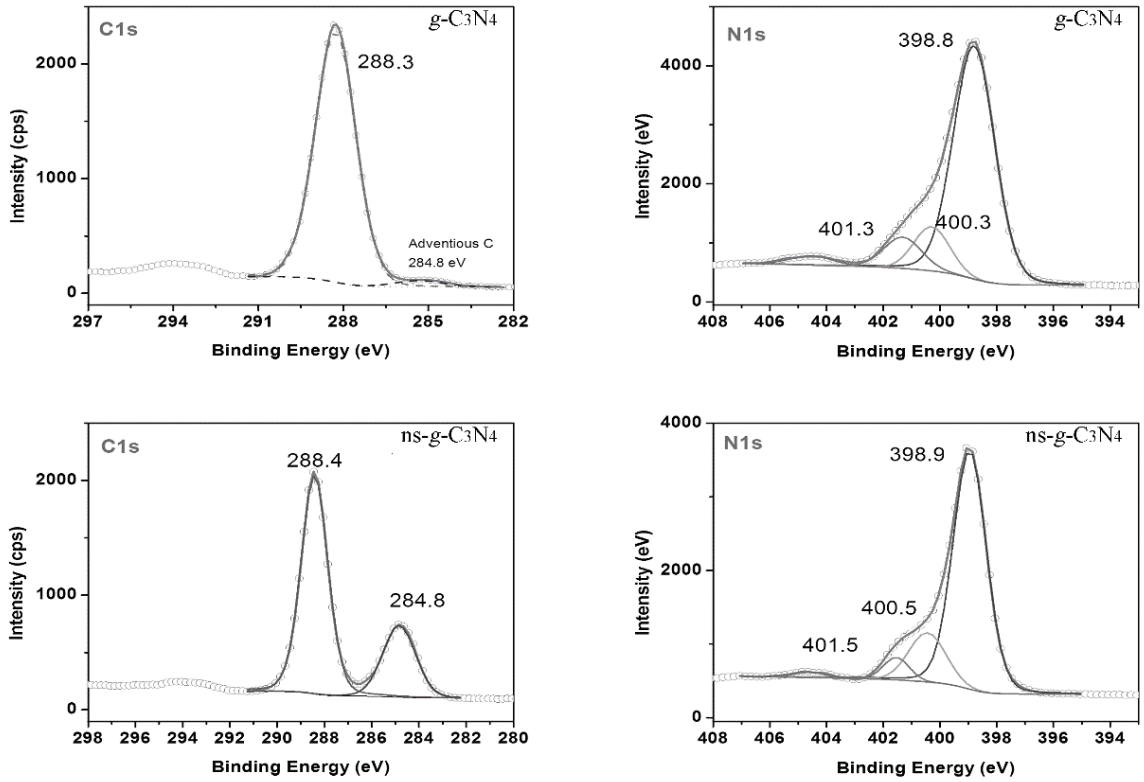

Figure 4: High resolution X-ray photoelectron spectra of *g*-C_3N_4 (top) and ns-*g*-C_3N_4 (bottom) samples of that were employed in this study. In both cases, the identified peaks are consistent with the chemical environments anticipated to be present in the layered carbon nitride structure.

The XPS spectra failed to show significant evidence of oxygen in the bulk samples of g-C_3N_4. Oxygen was detected in the nanostructured materials and the resulting O1s spectrum was de-convoluted into two peaks with binding energies of 532.6 eV and 533.9eV. The 532.6 eV peak

likely corresponds to surface hydroxyl groups of the silicon sample holder, while the 533.9eV peak corresponds to chemisorbed water molecules on the surface of the ns-*g*-C_3N_4 sample.[41] Importantly, the XPS spectrum of ns-*g*-C_3N_4 contains no evidence for either C-O or C=O species that would indicate partial oxidation of the *g*-C_3N_4 precursor.

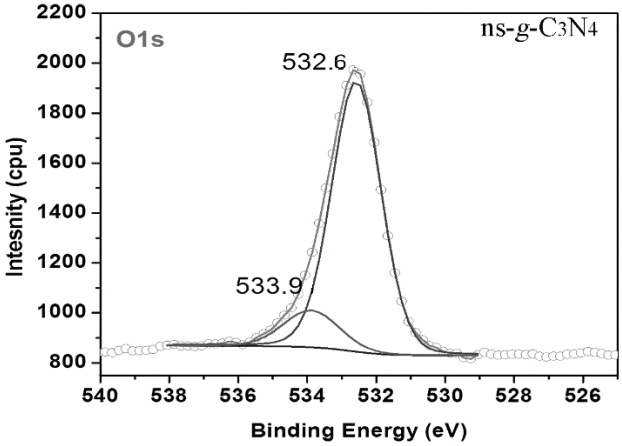

Figure 5: High resolution O1s X-ray photoelectron spectrum of bulk ns-*g*-C_3N_4.

Optical and Photochemical Properties of ns-*g*-C_3N_4

Samples of *g*-C_3N_4 are established intermediate band gap semiconductors.[42, 43] As determined by diffuse reflectance spectroscopy, the bulk and exfoliated samples of *g*-C_3N_4 both possess measured band gap energies of approximately 2.80 eV (Figure 6, *right*). The similarity in the optical properties of the materials reinforces the results of the XPS studies (Figure 4) and further indicates that no significant change in the chemical composition of the material occurred during the process of exfoliation.

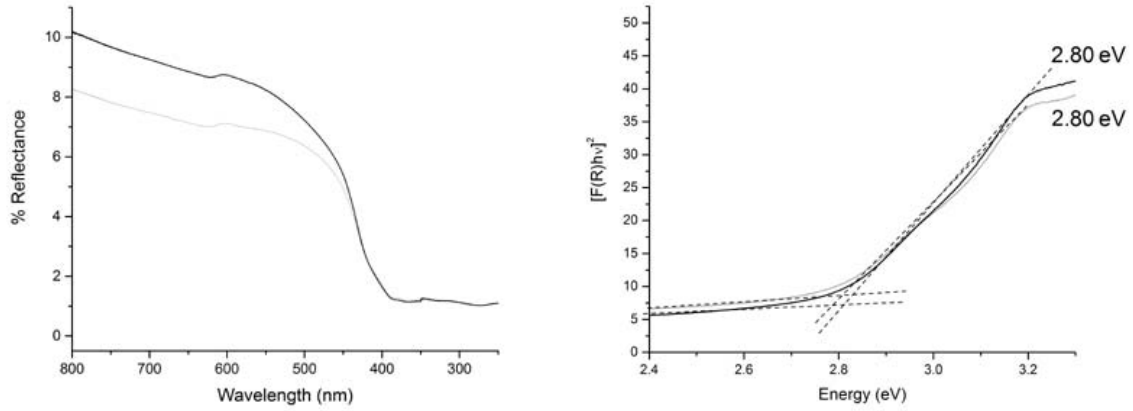

Figure 6: Diffuse reflectance UV-Vis spectrum (left) and calculated band gap energies (right) of samples of *g*-C_3N_4 (grey trace) and ns-*g*-C_3N_4 (black trace).

With respect to antimicrobial applications, the ability of a semiconductor to produce ROS is of fundamental importance.[44] The superoxide radical anion is likely the initial species that will be produced from the photochemical reduction of molecular oxygen.[45] This complex is highly reactive in aqueous solution and produces a number of additional ROS, including hydrogen peroxide (H_2O_2), the hydrogen peroxyl radical ($HO_2^{\bullet}$) and hydroxyl radical ($HO^{\bullet}$) (Equation 5). [15]

$$O_2 \rightarrow O_2^{-\bullet} \leftrightarrow HO_2^{\bullet} \rightarrow H_2O_2 \leftrightarrow HO^{\bullet} \qquad \text{Equation 5}$$

All ROS cause significant damage to cellular components of microorganisms and are potentially cytotoxic.[46] While it is clear that *g*-C_3N_4 does not contain the ionic bonding that typifies many traditional semiconducting materials, it is reported that the reduction potential of the conduction band of *g*-C_3N_4 can be estimated using Equation 6:[38]

$$E_{CB}^{0} = X - E^{C} - \frac{1}{2}E_g \qquad \text{Equation 6}$$

In this case, X is the geometric mean of the electronegativity of the constituent atoms of the semiconductor material (calculated to be 4.73 eV[47] for g-C_3N_4), E^C is a scaling factor that relates

the absolute vacuum scale to the normal hydrogen scale (~4.5 eV), and E_g is the experimentally determined band gap energy of the material. The calculated conduction band and valence band edge potentials for ns-*g*-C_3N_4 are -1.17 V and 1.63V, respectively. The conduction band edge reduction potential of ns-*g*-C_3N_4 is more negative than both the standard redox potential of molecular oxygen ($O_2/O_2^{-}\bullet$, E° = -0.33V) and the redox potential of a 1M aqueous solution of dioxygen ($O_2/O_2^{-}\bullet$, E° = -0.16V).[45] Consequently, it is possible to conclude that the materials used in this study have sufficient reducing power to promote the photochemical conversion of surface adsorbed oxygen molecules into ROS under appropriate experimental conditions.

We have confirmed the photochemical behavior of ns-*g*-C_3N_4 using the established, selective hydroxyl radical scavenging molecule coumarin-3-carboxylic acid (3-CCA).[48] In solution, reaction of 3-CCA with hydroxyl radicals produces the highly fluorescent molecule 7-hydroxycoumarin-3-carboxylic acid. As illustrated in Figure 7, irradiated reaction mixtures of ns-*g*-C_3N_4 and 3-CCA produced 7-hydroxycoumarin-3-carboxylic acid and a concomitant increase in fluorescence. In contrast, non-irradiated sample mixtures, or irradiated samples containing only ns-*g*-C_3N_4 or only 3-CCA, showed no observable change in the fluorescence. While direct oxidation of 3-CCA is theoretically possible, we anticipate that the Cl^- present in the reaction mixture will serve to trap the photogenerated holes and favor ROS production by means of reduction of surface adsorbed dioxygen.[49] These results indicate that ns-*g*-C_3N_4 successfully reduced molecular oxygen to produce cytotoxic ROS in the presence of visible radiation.

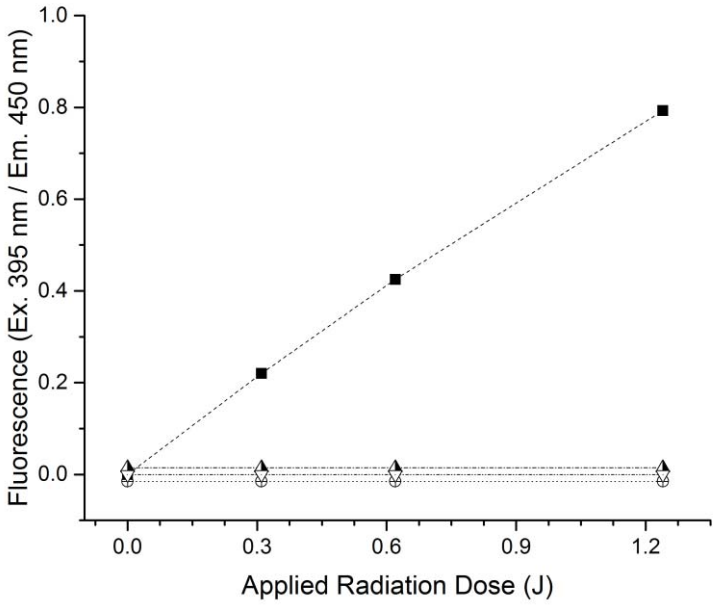

Figure 7: Observed change in fluorescence (λ_{ex} = 395 nm; λ_{em} = 450 nm) in mixtures of 3-CCA and ns-*g*-C_3N_4 with (---■---) and without (···⊕···) irradiation with visible light (400nm ≤ λ ≤ 442nm). Control reactions contained either irradiated 3-CCA alone (···▽···) or irradiated ns-*g*-C_3N_4 alone (---▲---).

Irradiated filters containing co-deposited samples of ns-*g*-C_3N_4 and either gram negative *E. coli* O157:H7 (Figure 8, *left*) or gram positive *S. aureus* (Figure 8, *right*) showed dramatic decreases in bacterial survivorship. In contrast, non-irradiated filters with co-deposited ns-*g*-C_3N_4 and bacterial cells (dark controls), and irradiated/non-irradiated filters containing only bacterial cells (no ns-*g*-C_3N_4) failed to impact bacterial survival. In the presence of ns-*g*-C_3N_4, irradiation with a 0.31J dose of visible light killed 49.4 ± 2.8% of *E. coli* O157:H7 cells, while a dose of 0.62J destroyed 97.1 ± 2.4% of the available CFUs (D-value = 112 min). Similarly, a total of 40.9 ± 3.4% of the available *S. aureus* CFUs were destroyed with a dose of 0.31J of visible radiation, while 93.7 ± 2.7% were eradicated with the 0.62J dose (D-value = 117 min).

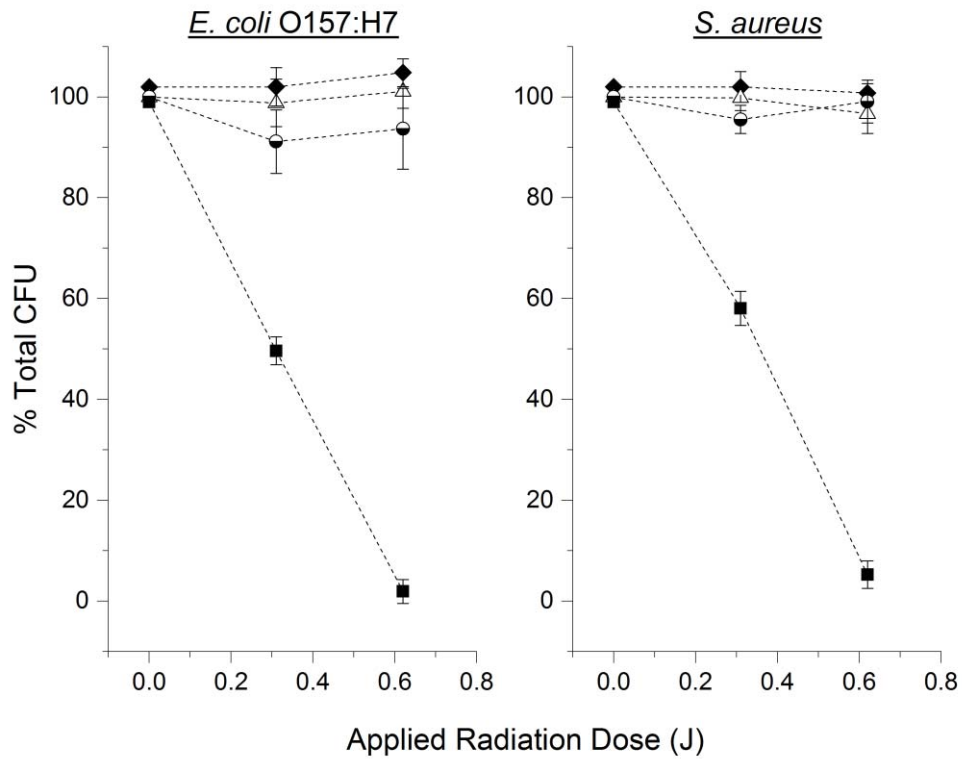

Figure 8: Relative number of CFUs (----■----) of *E. coli* O157:H7 or *S. aureus* observed as a function of applied radiation dose (400nm ≤ λ ≤ 442nm). Traces for dark control studies conducted with (----◒----) or without (----◆----) ns-*g*-C_3N_4, or irradiated without ns-*g*-C_3N_4 (----△----) are also presented. Error bars represent the standard error of the mean for three independent trials.

The results of the experiments described here indicate that the photoactive ns-*g*-C_3N_4 materials are not inherently toxic, nor is the observed antimicrobial activity simply a product of electromagnetic radiation-induced cellular damage.

The materials derived from *g*-C_3N_4 that are presented in this manuscript represent a specific advance in the development of antimicrobial surface coatings. Primarily, we note that the *g*-C_3N_4-films described in this study are photoresponsive to visible radiation. This stands in contrast to the highly energetic UV radiation required to drive wide band gap photocatalysts such as anatase TiO_2 and allows *g*-C_3N_4 to potentially function as antimicrobial and environmental remediation agents in interior environments without the need for potentially damaging radiation or cocatalysts.

Additionally, it is important to emphasize that the materials that we have developed in this study are able to achieve comparable and, in some cases superior, results for surface disinfection when challenged with either *E. coli* O157:H7 or *S. aureus*, relative to what has been reported for other semiconducting antimicrobial surface coatings.[50-53] The advantages of these *g*-C_3N_4-based materials over other, previously reported systems are observed both in terms of the relative required exposure time and in terms of the total reduction in CFU and are realized despite the fact that higher energy, UV radiation was employed in many of the earlier disinfection studies.

The composition of the *g*-C_3N_4 films that were used in this study presents another specific advantage. The lack of metals - especially copper and silver salts - in *g*-C_3N_4 is anticipated to increase the overall biological compatibility of this material, while the extended, polymeric structure may also act to suppress unwanted leaching and environmental redistribution. Lastly, we note that the *g*-C_3N_4 polymer is readily prepared in large scale from inexpensive, commercially available precursors. These properties suggest that films and coatings derived from *g*-C_3N_4 may find application in a hospital environment for the decontamination of surfaces with high touch frequency, including bed rails, countertops and door knobs, among others.

Conclusion

The intermediate band gap metal-free semiconductor ns-g-C_3N_4 was synthesized from bulk samples of carbon nitride *via* a simple exfoliation procedure. Fluorescent studies using 3-CCA indicate that irradiated samples of ns-*g*-C_3N_4 efficiently produce ROS. Films containing ns-*g*-C_3N_4 material showed biocidal activity against both gram negative and gram positive bacteria when exposed to visible radiation. Importantly, no antimicrobial activity was observed for ns-*g*-C_3N_4-based films that were not exposed to visible radiation, indicating that the materials developed for this study are not themselves inherently toxic. Ultimately, this work demonstrates that photoactive

ns-*g*-C_3N_4 is a promising candidate for a variety of biocidal and environmental remediation applications.

Corresponding Author

*Author to be contacted for correspondence: email: jthurston@collegeofidaho.edu, phone: (208)459-5531, fax: (208)459-5175

Acknowledgements

The work described in this publication was made possible by an Institutional Development Award (IDeA) from the National Institute of General Medical Sciences of the National Institutes of Health under Grants #P20GM103408 and #P20GM19095. We also acknowledge support from The Biomolecular Research Center at Boise State with funding from the National Science Foundation, Grants # 0619793 and #0923535; the MJ Murdock Charitable Trust; and the Idaho State Board of Education.

The authors thank Dr. Madhu Kongara and Prof. Alex Punnoose at Boise State University for help with the collection and analysis of the XPS and DRFTS data. Drs. Rick Ubrick and Karthik Chinnathambi (Boise State Center for Materials Characterization) are gratefully acknowledged for assistance with the collection and processing of electron microscopy and powder x-ray diffraction data.

The contents of this manuscript are solely the responsibility of the authors and do not necessarily represent the official views of NIH.

REFERENCES

1. E. Zimlichman, D. Henderson, O. Tamir, C. Franz, P. Song, C. K. Yamin, C. Keohane, C. R. Denham and D. W. Bates, *JAMA Int. Med.*, 2013, **173**, 2039.
2. B. Hota, *Clin Infect Dis*, 2004, **39**, 1182-1189.
3. A. Kramer, I. Schwebke and G. Kampf, *BMC Infect. Dis.*, 2006, **6**, 130-130.
4. J. M. Boyce, *J. Hosp. Infect.*, 2007, **65, Supplement 2**, 50-54.
5. R. Dastjerdi and M. Montazer, *Colloid Surface B*, 2010, **79**, 5-18.
6. G. Fu, P. S. Vary and C.-T. Lin, *J. Phys. Chem. B*, 2005, **109**, 8889-8898.
7. M. Rai, A. Yadav and A. Gade, *Biotechnol. Adv.*, 2009, **27**, 76-83.
8. Y. Zhang, M. Ding, L. Zhou, H. Tan, J. Li, H. Xiao, J. Li and J. Snow, *Polym. Chem.*, 2012, **3**, 907-913.
9. E.-R. Kenawy, S. D. Worley and R. Broughton, *Biomacromolecules*, 2007, **8**, 1359-1384.
10. G. Ye, J. Lee, F. Perreault and M. Elimelech, *ACS Appl. Mater. Interfaces*, 2015, **7**, 23069-23079.
11. K. M. Xiu, Q. Cai, J. S. Li, X. P. Yang, W. T. Yang and F. J. Xu, *Colloid Surface B*, 2012, **90**, 177-183.
12. I. Banerjee, D. Mondal, J. Martin and R. S. Kane, *Langmuir*, 2010, **26**, 17369-17374.
13. X. Dong, E. McCoy, M. Zhang and L. Yang, *J. Environ. Sci.*, 2014, **26**, 2526-2534.
14. A. Lovo de Carvalho, B. F. Ferreira, C. H. G. Martins, E. J. Nassar, S. Nakagaki, G. S. Machado, V. Rives, R. Trujillano, M. A. Vicente, A. Gil, S. A. Korili, E. H. de Faria and K. J. Ciuffi, *J. Phys. Chem. C*, 2014, **118**, 24562-24574.
15. M. R. Hoffmann, S. T. Martin, W. Choi and D. W. Bahnemannt, *Chem. Rev.*, 1995, **95**, 69-96.
16. K. Page, M. Wilson and I. P. Parkin, *J. Mater. Chem.*, 2009, **19**, 3819-3831.
17. F. Dong, Z. Zhao, Y. Sun, Y. Zhang, S. Yan and Z. Wu, *Environ. Sci. Technol.*, 2015, **49**, 12432-12440.
18. N. Tian, H. Huang, C. Liu, F. Dong, T. Zhang, X. Du, S. Yu and Y. Zhang, *J. Mater. Chem. A*, 2015, **3**, 17120-17129.
19. J. Wen, X. Li, H. Li, S. Ma, K. He, Y. Xu, Y. Fang, W. Liu and Q. Gao, *Appl. Surf. Sci.*, 2015, **358, Part A**, 204-212.
20. Z. Zhao, Y. Sun and F. Dong, *Nanoscale*, 2015, **7**, 15-37.
21. Y. Shiraishi, S. Kanazawa, Y. Sugano, D. Tsukamoto, H. Sakamoto, S. Ichikawa and T. Hirai, *ACS Catal.*, 2014, **4**, 774-780.
22. S. C. Yan, Z. S. Li and Z. G. Zou, *Langmuir*, 2009, **25**, 10397-10401.
23. Y. Tian, B. Chang, J. Lu, J. Fu, F. Xi and X. Dong, *ACS Appl. Mater. Inter.*, 2013, **5**, 7079-7085.
24. J. Zhu, P. Xiao, H. Li and S. A. C. Carabineiro, *ACS Appl. Mater. Inter.*, 2014, **6**, 16449-16465.
25. S. Zhang, J. Li, M. Zeng, G. Zhao, J. Xu, W. Hu and X. Wang, *ACS Appl. Mater. Inter.*, 2013, **5**, 12735-12743.
26. W. Wang, J. C. Yu, D. Xia, P. K. Wong and Y. Li, *Environ. Sci. Technol.*, 2013, **47**, 8724-8732.
27. Y. Li, L. Fang, R. Jin, Y. Yang, X. Fang, Y. Xing and S. Song, *Nanoscale*, 2015, **7**, 758-764.
28. J. Huang, W. Hoc and X. Wang, *Chem. Comm.*, 2014, **50**, 4338-4340.

29. H. Zhao, H. Yu, X. Quan, S. Chen, Y. Zhang, H. Zhao and H. WangKey, *Appl. Catal. B-Environ.*, 2014, **152-153**, 46-50.
30. J. Liu, T. Zhang, Z. Wang, G. Dawson and W. Chen, *J. Mater. Chem.*, 2011, **21**.
31. S. Yang, Y. Gong, J. Zhang, L. Zhan, L. Ma, Z. Fang, R. Vajtai, X. Wang and P. M. Ajayan, *Adv. Mater.*, 2013, **25**, 2452-2456.
32. P. Kubelka and F. Munk, *Z. Tech. Phys.*, 1931, **12**, 593-601.
33. J. Shi, L. Ma, P. Wu, Z. Zhou, J. Jiang, X. Wan, D. Jing and L. Guo, *ChemCatChem*, 2012, **4**, 1389-1396.
34. Y. Manevich, K. D. Held and J. E. Biaglow, *Radiat. Res.*, 1997, **148**, 580-591.
35. M.-S. Wong, D.-S. Sun and H.-H. Chang, *PLoS ONE*, 2010, **5**, e10394.
36. W. A. Rutala, E. B. Katz, R. J. Sherertz and F. A. Sarubbi, *J. Clin. Microbiol.*, 1983, **18**, 683-688.
37. D. Mulvey, P. Redding, C. Robertson, C. Woodall, P. Kingsmore, D. Bedwell and S. J. Dancer, *J. Hosp. Infect.*, 2011, **77**, 25-30.
38. N. Boonprakob, N. Wetchakun, S. Phanichphant, D. Waxler, P. Sherrell, A. Nattestad, J. Chen and B. Inceesungvorn, *J Colloid Interf. Sci*, 2014, **417**, 402-409.
39. X. Bai, L. Wang, R. Zong and Y. Zhu, *J. Phys. Chem. C*, 2013, **117**, 9952-9961.
40. F. Yang, V. Kuznietsov, M. Lublow, C. Merschjann, A. Steigert, J. Klaer, A. Thomase and T. Schedel-Niedriga, *J. Mater. Sci. A*, 2013, **1**, 6407-6415.
41. Y. L. Khung, S. H. Ngalim, A. Scaccabarozzi and D. Narducci, *Beilstein J Nanotechnol*, 2015, **6**, 19-26.
42. G. Dong, Y. Zhang, Q. Pan and J. Qiu, *J. Photoch. Photobio. C.*, 2014, **20**, 33-50.
43. X. Wang, K. Maeda, A. Thomas, K. Takanabe, G. Xin, J. M. Carlsson, K. Domen and M. Antonietti, *Nat Mater*, 2009, **8**, 76-80.
44. K. Datta, S. Sinha and P. Chattopadhyay, *Natl. Med. J. India*, 2000, **13**, 304-310.
45. P. M. Wood, *Biochem J.*, 1988, **253**, 287-289.
46. E. Cabiscol, J. Tamarit and J. Ros, *Int. Microbiol.*, 2000, **3**, 3-8.
47. J. Zhang, Y. Hu, X. Jiang, S. Chen, S. Meng and X. Fu, *J Hazard Mater*, 2014, **280**, 713-722.
48. Q. Xiang, J. Yu and P. K. Wong, *J. Colloid Interf. Sci*, 2011, **357**, 163-167.
49. X. Zhang, H. Cui, M. Humayun, Y. Qu, N. Fan, X. Sun and L. Jing, *Sci. Rep.*, 2016, **6**, 21430.
50. J. C. Yu, W. Ho, J. Lin, H. Yip and P. K. Wong, *Environ. Sci. Technol.*, 2003, **37**, 2296-2301.
51. P. S. M. Dunlop, C. P. Sheeran, J. A. Byrne, M. A. S. McMahon, M. A. Boyle and K. G. McGuigan, *J. Photoch. Photobio. A.*, 2010, **216**, 303-310.
52. A. Erkan, U. Bakir and G. Karakas, *J Photoch. Photobio. A*, 2006, **184**, 313-321.
53. M. Wakamura, K. Hashimoto and T. Watanabe, *Langmuir*, 2003, **19**, 3428-3431.